Sustainable Polymer & Energy

SCIEPublish

Article

Transition from Dispersed RTP to Aggregated TADF in Single-Chromophore Polymers

Hanyu Wang [1,†], Yan Guan [2,†], Yang Wang [3], Chengheng Wu [1], Ping Wang [1,*] and Fuzhi Wang [3,*]

[1] Key Laboratory of Advanced Functional Polymer Materials of Colleges and Universities of Hunan Province, Key Laboratory of Polymeric Materials and Application Technology of Hunan Province, Key Laboratory of Environment-Friendly Chemistry and Application of the Ministry of Education, College of Chemistry, Xiangtan University, Xiangtan 411105, China; 202321531781@smail.xtu.edu.cn (H.W.); 202321531784@smail.xtu.edu.cn (C.W.)

[2] Beijing National Laboratory for Molecular Sciences, Key Laboratory of Polymer Chemistry and Physics of Ministry of Education, Center for Soft Matter Science and Engineering, College of Chemistry and Molecular Engineering, Peking University, Beijing 100871, China; yanguan@pku.edu.cn (Y.G.)

[3] State Key Laboratory of Alternate Electrical Power System with Renewable Energy Sources, School of New Energy, North China Electric Power University, Beijing 102206, China; 120242111041@ncepu.edu.cn (Y.W.)

* Corresponding author. E-mail: wangping01@xtu.edu.cn (P.W.); wfz501@ncepu.edu.cn (F.W.)

† These authors contributed equally to this work.

Received: 9 April 2026; Revised: 29 April 2026; Accepted: 8 May 2026; Available online: 18 May 2026

ABSTRACT: Room temperature phosphorescence (RTP) and organic thermally activated delayed fluorescence (TADF) materials have merited enormous application prospects in organic optoelectronics. In spite of this, TADF and RTP dual emissions based on single-chromophore polymers still face a great challenge. In this work, we develop a monomer (CzBT) with twisted electron donating carbazole and electron withdrawing benzothiadiazole (D-A) structure and then copolymerize it with *N*-isopropylacrylamide (NIPAM) in different ratios to adjust TADF and RTP emission. The polymers exhibit TADF emission from aggregated chromophores, RTP emission with a lifetime of 240 ms from dispersed chromophores, and a high absolute photoluminescence quantum efficiency (20%). Theoretical calculations confirm that the introduction of twisted D-A structure and heteroatoms can not only promote spin orbital coupling to facilitate the accumulation of triplet excitons for RTP emission, but also help RISC to emit TADF in the aggregated state. When applied to solution-processable organic light emitting diodes (OLEDs) devices, excellent current efficiency of 62.7 cd/A and maximum external quantum efficiency of 19.9% were achieved attributing to the dominant TADF emission. This class of polymers paves the way for high-efficiency optoelectronic devices.

Keywords: Thermally activated delayed fluorescence (TADF); Room temperature phosphorescence (RTP); Organic light emitting diode (OLED); Dual emissions

1. Introduction

Organic room temperature phosphorescence (RTP) and thermally activated delayed fluorescence (TADF) materials have gained enormous attention in recent years as they can achieve theoretically 100% quantum efficiency by utilization of triplet exciton and long-lived lifetime without the need of rare earth

metal complexes [1–8]. Since Adachi and co-workers developed the organic TADF emitters based on carbazolyl dicyanobenzene and applied them to organic light-emitting diodes (OLEDs) [9], TADF emitters have gained significant progress in OLEDs, and various TADF materials have been developed to obtain high efficiency devices for displays and solid state lighting [10–15]. For effective TADF emission, the small energy gap (ΔE_{ST}) is advantageous for the exciton to transition from triplet to singlet states via an effective reverse inter-system crossing (RISC) process, which is often obtained through separating the spatial wave functions of the highest occupied molecular orbital (HOMO) and the lowest unoccupied molecular orbital (LUMO). In terms of molecular structure design, TADF molecules generally adopt the twisted donor-acceptor (D-A) structure, which presents intramolecular charge transfer (ICT) characteristics and will lead to separated HOMO and LUMO distributions and thereby small ΔE_{ST} [16–20]. Regarding RTP, various approaches have been proposed to promote spin orbital coupling (SOC) between singlet and triplet states through introducing heavy atoms, heteroatoms, aromatic carbonyl compounds, and so on [21,22]. Besides, varied methods such as crystallization [23], supramolecular assembly [24], host-guest doping [25], and polymer confinement [26,27] are always used to stabilize triplet excitons and suppress nonradiative decay of triplet excitons for achieving RTP, among which polymer confinement has significant advantages due to its flexibility and processability. In the past decade, organic materials with TADF and RTP dual emissions were mainly achieved through host-guest doping and crystal engineering [28–35]. Recently, Gather et al. [29] developed a family of nitrogen-containing indolocarbazoles, two of which exhibited multi-resonant TADF and RTP biluminescence when doped in PMMA at 1 wt% concentration. A series of triphenylamine-substituted isoquinoline derivatives with monomeric TADF and aggregated RTP were reported by Ma et al. [35]. Nevertheless, achieving both TADF and RTP emission remains a huge challenge, especially in non-doped polymers.

In this work, we propose to introduce twisted D-A structure (carbazole as the electron-donor and benzo-2,1,3-thiadiazole as the electron-acceptor) to the side group of the monomer (CzBT) and copolymerize it with NIPAM in different proportions through photopolymerization to obtain polymers (NP1-10~NP1-1000) (Scheme 1). The twisted D-A structure and the heteroatoms (S, N) would promote the SOC and provide appropriate ΔE_{ST} for the moderate RISC process. The dual cross-linked networks formed by photopolymerization of NIPAM could immobilize and accumulate the triplet excitons [36]. The copolymerization ratios could adjust the stability of triplet excitons, thereby affecting their emission channels. As expected, both TADF emission and RTP with a hundred-millisecond level lifetime and up to 20% absolute photoluminescence quantum efficiency were achieved. Importantly, the solution-processable OLED device with CzBT doping in PVK as the light emitting layer presented excellent current efficiency (62.7 cd/A) and high luminance (90,858 cd/m^2). This work presents potential applications in high performance optoelectronics.

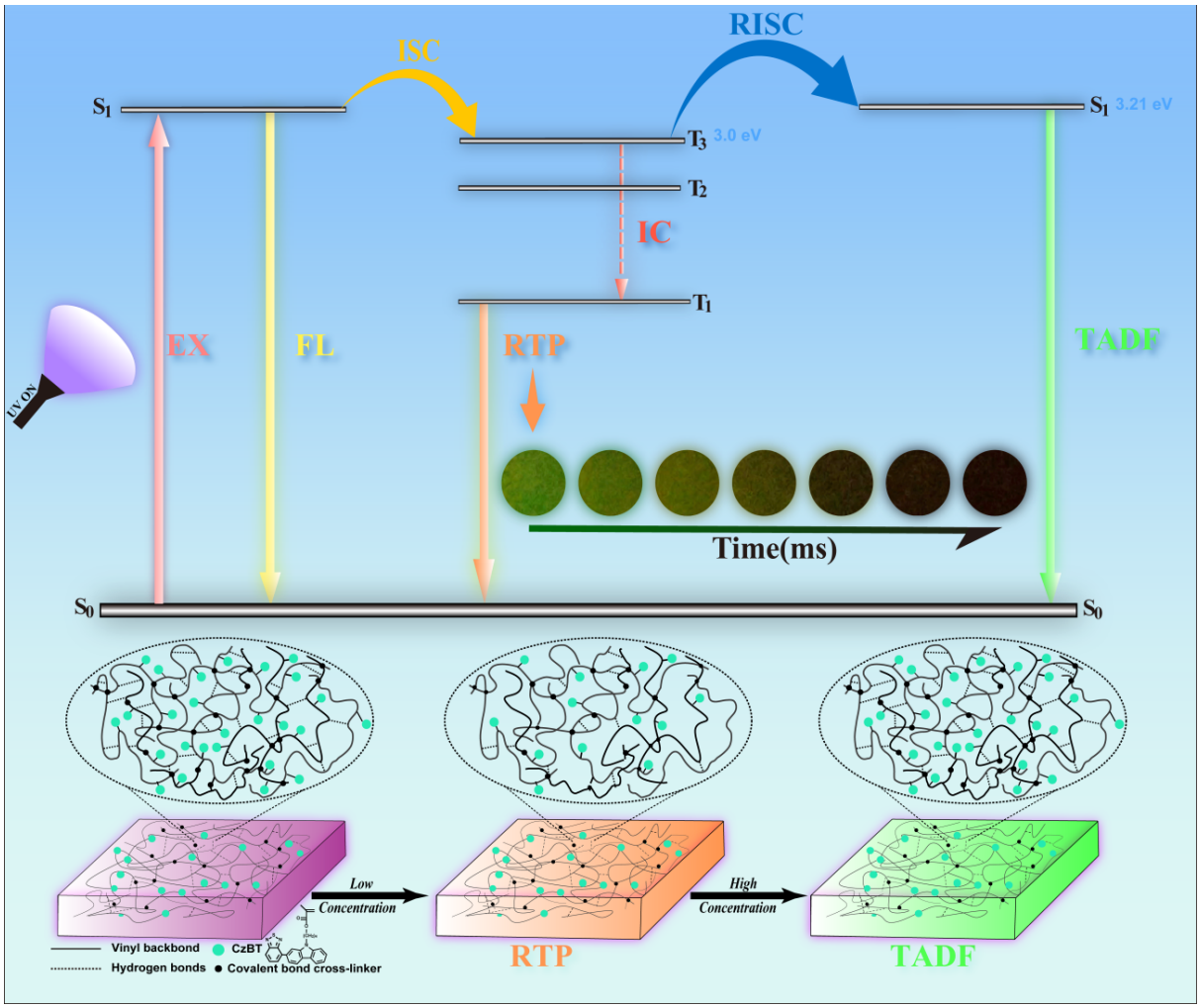

Scheme 1. Proposed TADF and RTP dual emission mechanism for polymers NP1-10~NP1-1000.

2. Results and Discussion

2.1. The Characterization of Monomers and Polymers

The monomer CzBT was prepared mainly by Suzuki coupling reactions, the monomer NIPAM was purchased and used after recrystallization. The structure characterizations of the monomer were identified by ^{1}H NMR, ^{13}C NMR, MALDI-TOF, and HPLC spectra. Specific synthetic routes and characterization results were included in the supporting information (Scheme S1 and Figures S1–S5). The ^{1}H NMR spectra (Figure 1a) illustrated that chemical shift peaks at 8.27–7.21 ppm were attributed to aromatic hydrogen, while the chemical shift peaks at 5.88 and 5.52 ppm belonged to hydrogen on the double bond. The ^{13}C NMR and MALDI-TOF spectra of CzBT further indicated that the monomer was successfully synthesized. The single peak in the HPLC spectra (Figure S4) of CzBT indicated the high purity. The polymers (NP1-50~NP1-1000) were obtained by free radical photopolymerization of monomer CzBT and NIPAM in different ratios (CzBT:NIPAM = 1:10, 1:50, 1:100, 1:200, 1:500 and 1:1000). The FTIR spectra (Figures 1b and S5) disclosed that the strong sharp absorbance at 3280 cm^{-1} attributed to the free -NH stretching vibration of NIPAM converted to broad stretching vibration bands for polymer NP1-50, which was due to the formation of amount of hydrogen bondings. The absorption band at 1265 cm^{-1} was attributed to the stretching vibration of C-N in CzBT, and the disappearance of the 810 cm^{-1} peak belonging to the out-of-plane bending vibration of C=C-H in NIPAM further proved the successful synthesis of the polymers. The molecular weight data of polymers are revealed in Table S1. The thermogravimetric analysis and differential scanning calorimetry (Figures S6 and S7) results suggested good thermal stability.

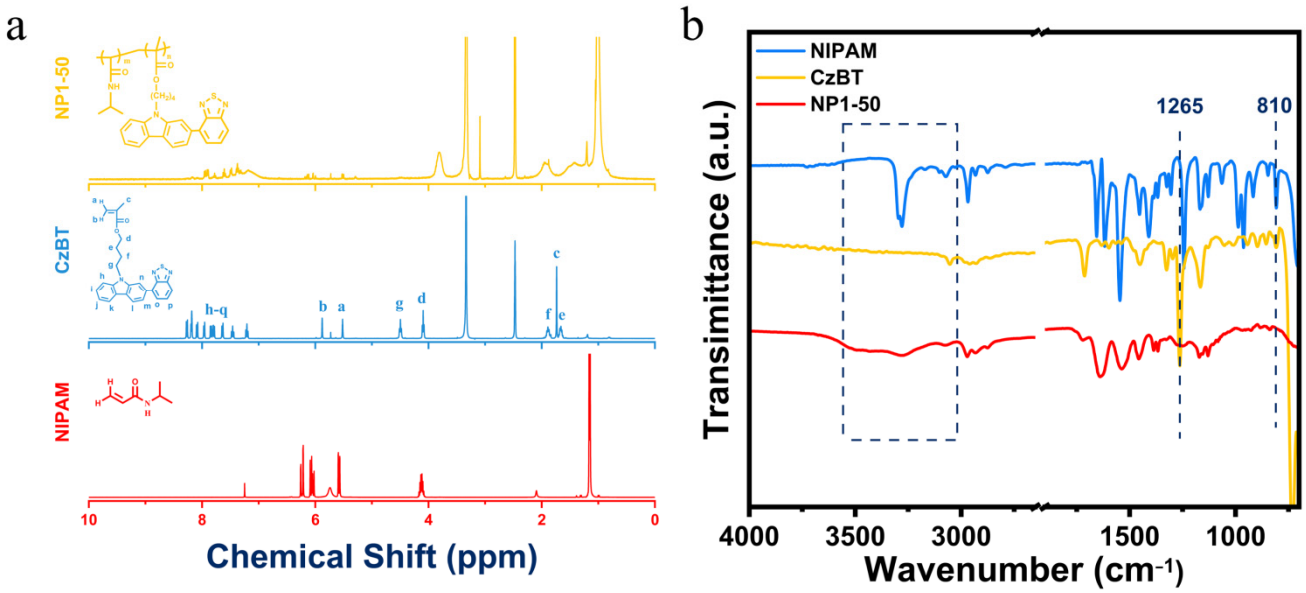

Figure 1. The ^{1}H NMR (**a**) and FTIR spectra (**b**) of monomer and polymers.

2.2. Photophysical Properties of the Monomer CzBT

The absorption spectra of CzBT in dichloromethane dilute solutions are illustrated in Figure 2a. The maximum absorption at 304 nm and 370 nm for CzBT were attributed to the π-π* electronic transition and intramolecular charge transfer (ICT) transitions, respectively. From the maximum fluorescent emissions and delayed emission (77 K) of monomer CzBT with relatively large energy gaps, we assume that the weak emission at 500 nm in the delayed spectrum at 77 K is attributed to the triplet-triplet annihilation [37]. Moreover, the fluorescent emissions are solvent dependent (Figure 2b). The maximum fluorescent emission wavelength of CzBT in different polar solvents red-shifted from 484 nm to 610 nm with a strong excited-state solvatochromic effect. The maximum emission wavelength increased as the solvent polarity increased, which indicated that CzBT possessed ICT from carbazole to the benzothiazole unit. It is obvious that the red-shift was ascribed to the stabilization of excited states by the polar solvent molecules. It has been demonstrated [38] that suppressing the ICT rotations through molecular aggregation could also stimulate aggregation induced emission (AIE) behavior. Thus, we assumed that CzBT possessed AIE phenomenon. The AIE experiments with CzBT were performed in THF-water mixtures with varying volume fractions, as shown in Figure 2c. At a lower fraction of water (<70%), the fluorescent emission intensities of CzBT were similar to that of in pure THF. As the water fraction increased from 70% to 90%, significant increase were observed with nearly 18-fold enhancement compared with that of in pure THF. It is clear that the AIE effect of CzBT would endow it with excellent emission performance in the solid state.

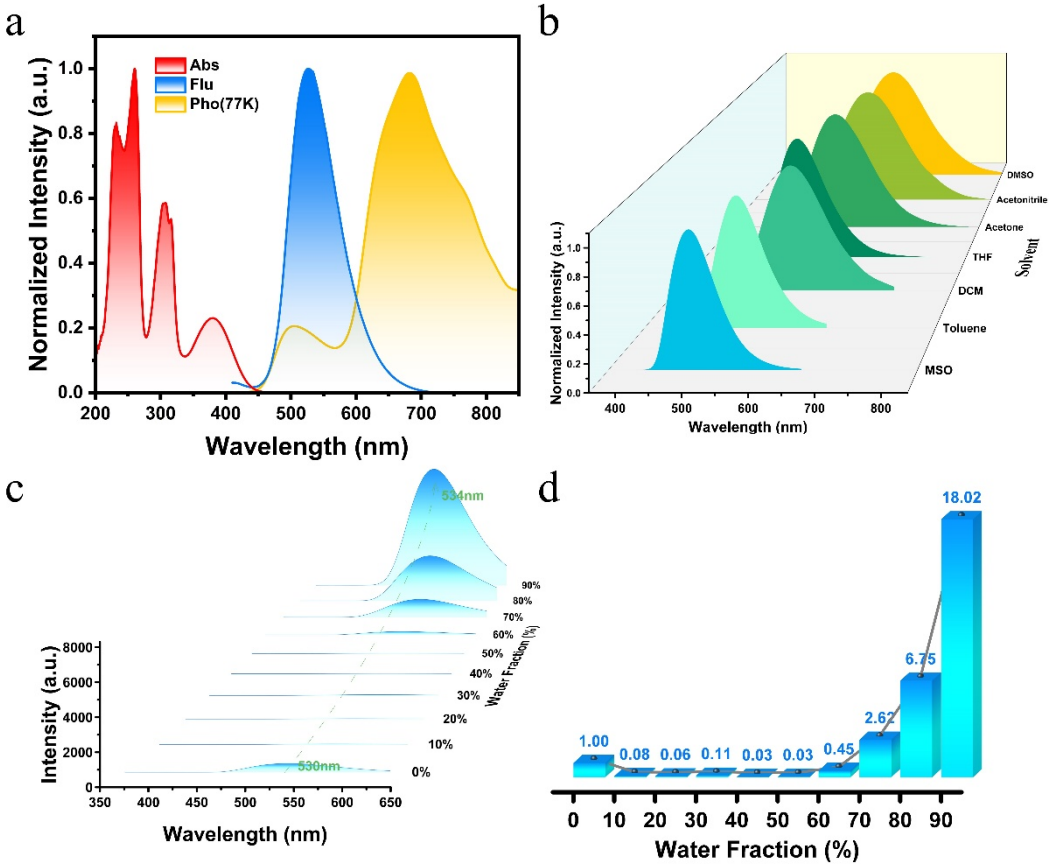

Figure 2. (**a**) The absorption, fluorescent, and delayed spectra (77 K) of monomer CzBT in solution; and (**b**) PL spectra in different polarity solvents; (**c**) PL spectra and plot of the maximum emission peak intensity (**d**) in THF and water mixtures with different water percentages.

2.3. Aggregated TADF and Dispersed RTP Emissions

Given the good AIE performance, the photophysical properties of polymers in films were illustrated in Figure 3. Upon excitation, all of the six polymers (NP1-10~NP1-1000) emitted single fluorescence emission with maximum emission wavelengths ranging from 500 nm to 510 nm for NP1-10~NP1-1000, which was similar to the PL spectra of monomer CzBT in solution (Figure 3). The fluorescent lifetimes (Table S2) of polymers are in the nanosecond level, which coincides with the nature of fluorescence. Importantly, when the experiments were performed in delayed mode (delay time 0.01 ms), all of the polymers manifested bright afterglows. Among them, NP1-10 displayed a broad delay peak located at 510 nm, which basically coincides with its fluorescence spectra. And dual emission bands located at around 510 nm and 630 nm were observed for polymers NP1-50~NP1-500, while only one delayed emission at 540 nm for polymer NP1-1000.

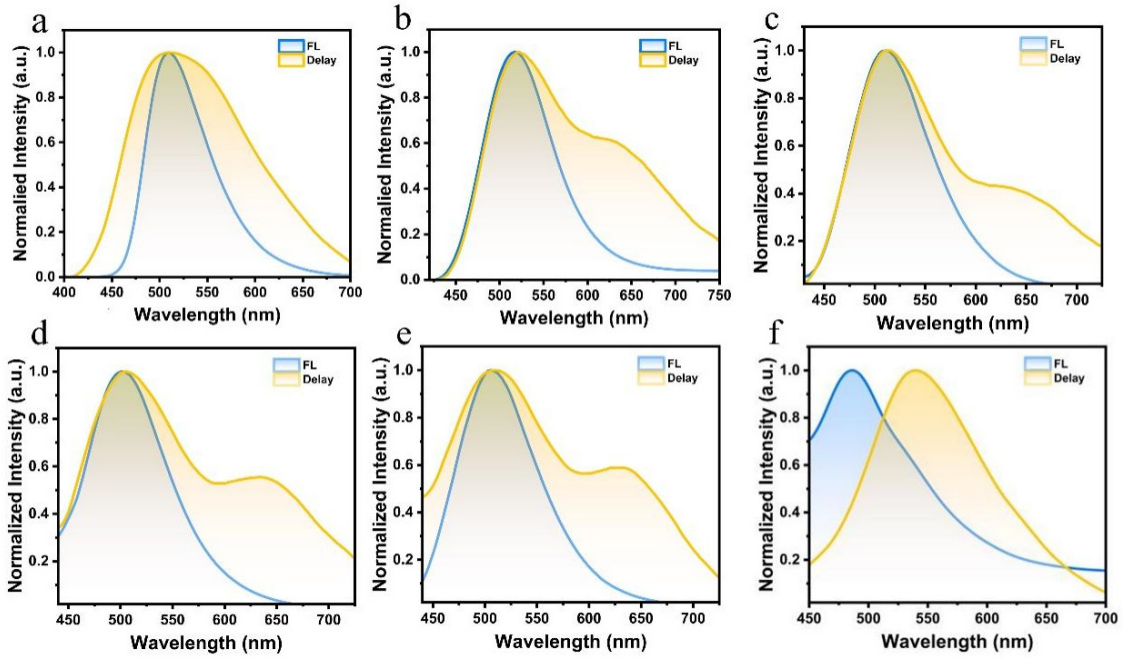

Figure 3. (**a**) Fluorescent and delayed spectra (Ex: 380 nm) of polymers NP1-10; (**b**) NP1-50; (**c**) NP1-100; (**d**) NP1-200; (**e**) NP1-500; (**f**) NP1-1000.

In order to clarify the attribution of the delay peaks mentioned above, the temperature-dependent delayed spectra of NP1-10 and NP1-1000 (Figure 4a,b) were conducted. The temperature-dependent delayed spectra of NP1-10 (Figure 4a) suggested that the delayed fluorescence intensity increased as the temperature increased from 77 K to 298 K, which confirmed the TADF characteristics of NP1-10 [39]. The microsecond level lifetime (14 μs, Figure 4c) further verified that the delayed emission of NP1-10 was attributed to TADF. Meanwhile, the delayed emission of monomer CzBT at 77 K and polymer NP1-100 suggested the RTP emission (Figure S8). In addition, the delayed emission intensity of polymer NP1-1000 and NP1-50 decreased with increasing temperature, further confirming the RTP emission (Figures 4b and S9). Moreover, the RTP emission displayed long-lived lifetimes ranging from 32 to 268 ms for the polymers (NP1-50~NP1-1000) at both two emission bands, which further revealed the RTP emission (Figure 4c and Table S2). In addition, the polymers exhibited typical excitation wavelength dependent phosphorescence emission characteristics. Taking NP1-50 as an example (Figure S10), when excited below 380 nm, it mainly exhibited phosphorescence emission below 540 nm. As the excitation wavelength increased, phosphorescence emission around 630 nm was enhanced. This may be due to the fact that the short wavelength phosphorescence emission mainly came from the contribution of the carbazole group, while the long wavelength emission was mainly attributed to the benzothiadiazole group. More importantly, the delayed spectra of the polymers (NP1-50~NP1-1000) with different concentrations were compared as shown in Figure S11. Due to its high concentration, NP1-50 exhibited two distinct phosphorescence emission peaks, and the peak at 630 nm was relatively high compared to other polymers. The yellow afterglow was due to the combined effect of the two peaks. While NP1-1000 mainly showed a phosphorescent peak around 540 nm due to its low concentration, it also displayed the delayed spectra of NP1-100-NP1-500 also presented two peaks, and the peak belonging to the green part was much stronger, thus mainly reflecting the green afterglow. From the afterglow CIE color coordinate graph (Figure 4d), it can be clearly seen the color-tunable phosphorescent emission from orange to yellow green for NP1-50~NP1-1000 with different feed ratios. Moreover, the color-tunable afterglow phenomenon can be observed from the delay time-dependent spectra and corresponding CIE chromatography, as shown in Figures 4e and S12. The afterglow photographs at different delay times further showed that visible

afterglows lasting for up to 2 s, accompanied by significant color changes (Figure 4g). It manifested that the dual emission features of the polymers enabled them to have color-tunable afterglows with feed ratios and delay time dependence. Additionally, all of the polymers illustrated high absolute photoluminescence quantum yields, with polymer NP1-200 reaching 20.4% (Figure 4f). All of the corresponding spectral, lifetime, and rate constants data have been summarized in Table S2. It was obvious that the introduction of D-A twisted structure realized high efficiency TADF and RTP dual emissions.

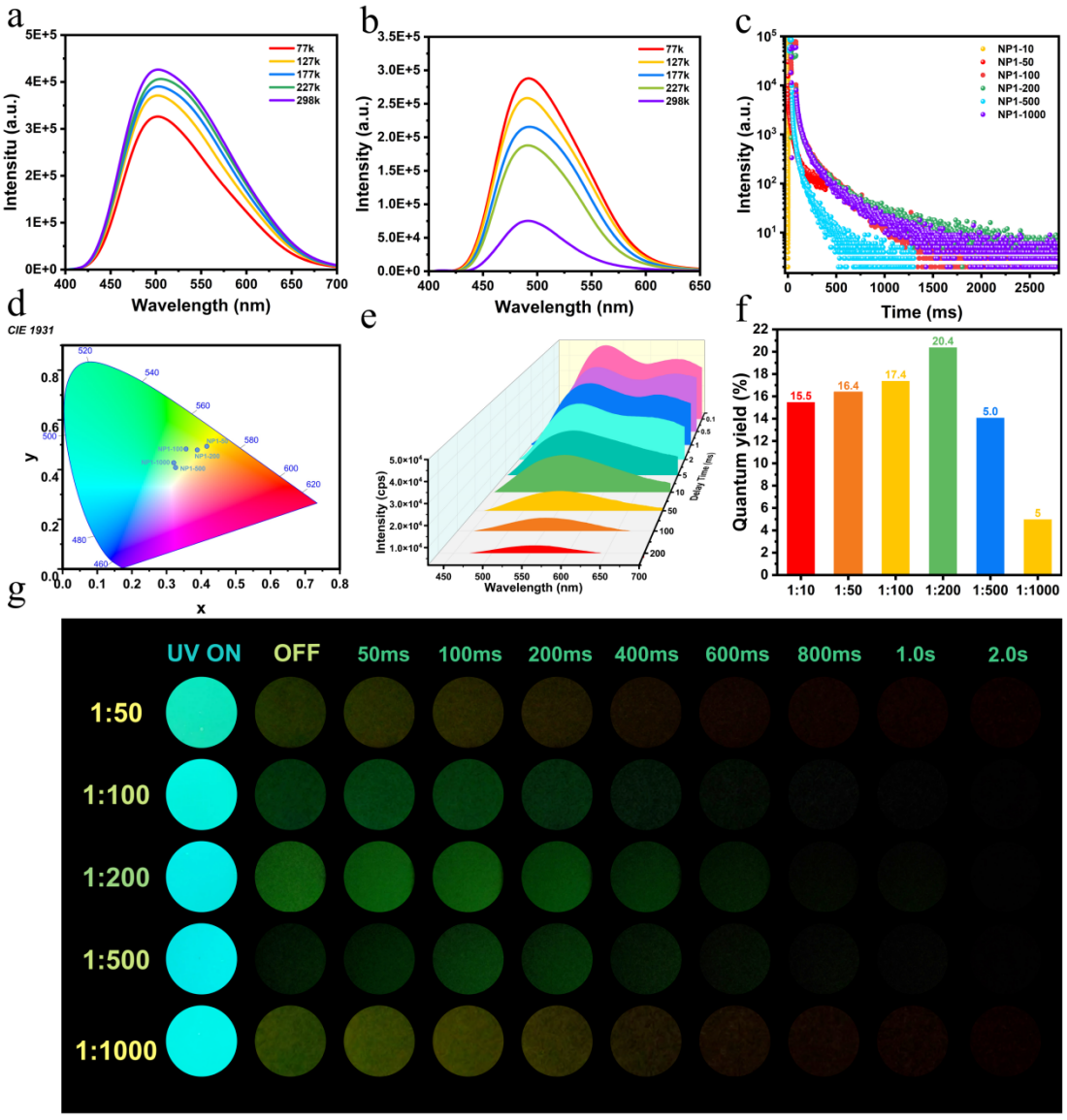

Figure 4. (**a**) Temperature-dependent delayed spectra of polymer NP1-10 and (**b**) NP1-1000; (**c**) Life time curves of polymers NP1-10~NP1-1000; (**d**) CIE coordinate diagrams of polymers; (**e**) Transient delay spectra of polymer NP1-200; (**f**) Quantum yield of polymers; (**g**) Afterglow photographs of polymers NP1-50~NP1-1000.

2.4. Mechanism Analysis of TADF and RTP Dual Emissions

To theoretically understand the photophysical properties of polymers, especially the TADF and RTP dual emission, the time-dependent density functional theory (TD-DFT) calculations were carried out with CAM-B3LYP/def2-svp level for monomer CzBT in the gas state. Firstly, the geometric structures of monomer CzBT in the S_0, S_1, and T_1 states (Figure 5) were optimized, and their electronic structure properties, including natural transition orbitals, vertical excitation energy, and spin orbital coupling (SOC) between the singlet and triplet states, were investigated carefully. As shown in Figure 5a, the HOMO of

CzBT exists on the whole molecule in S_1 and T_1 states, while the LUMO of CzBT resides mainly on the benzo-2,1,3-thiadiazole units due to their electron-deficient features. It can be seen that the dihedral angles (Figure 5c) are getting lower upon excitation in the S_0-S_1 and S_0-T_1 transitions, the more effective HOMO and LUMO differential overlap is beneficial for radiative decay from both S_1-S_0 and T_1-S_0 [40]. From the excited state energy level (Figure 5b), it can be found that CzBT has multiple SOC channels and a relatively large SOC value (0.4 cm^{-1}) between the S_1 and T_3 state. The large SOC value is beneficial for the exciton transition from singlet state S_1 to triplet state T_3 through intersystem crossing, followed by internal conversion to T_1 state, and then radiative transition to obtain RTP [41–43]. We speculate that in polymers (NP1-50~1-1000) with low concentration phosphors, the polymers can effectively fix and stabilize triplet excitons, which mainly exhibit RTP emission; In high concentration polymers (NP1-10), due to intermolecular interactions, the distribution of high-energy excited states can be altered [44], a large number of triplet excitons cannot be fixed and undergo RISC to S_1 state with the assistance of heat, resulting in delayed fluorescence, also known as TADF (Figure 5d). Here, we can infer that the molecular design of CzBT can not only promote SOC to facilitate the accumulation of triplet excitons for RTP emission, but also help RISC to emit TADF in the aggregated state.

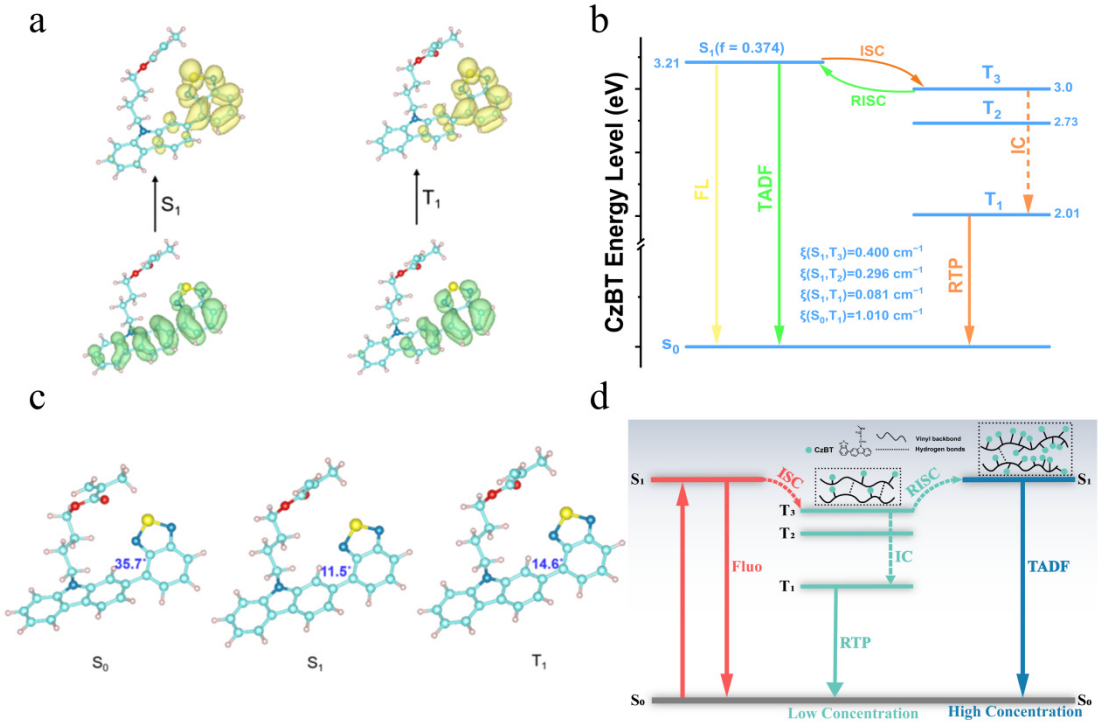

Figure 5. (**a**) Calculated transition orbitals of the S_1 and T_1 states at the optimized S_1 and T_1 geometries; (**b**) Calculated energy diagram and spin-orbital coupling (ξ) at the S_1-geometry; (**c**) The optimized geometric structures of CzBT; (**d**) Schematic diagram of the mechanism of TADF and RTP dual emissions.

2.5. Application in Solution-Processed OLEDs

Based on the excellent TADF and RTP dual emission properties of the aforementioned polymers, we intend to apply them to OLED devices. However, due to the poor solubility and conductivity of the polymers, we doped the monomer CzBT into polyvinycarbazole (PVK) and found that it still exhibited delayed emissions similar to the fluorescent spectra with maximum emission at 538 nm (Figure S13). The refractive index of CzBT:PVK (1:10) film was 1.57 at 565 nm. The relatively high refractive index indicates good light output coupling efficiency. TADF materials have significant advantages in achieving almost complete exciton utilization through RISC, which allows triplet excitons to transition from T_1 to S_1,

resulting in up to 100% theoretical internal quantum efficiency [44,45]. This characteristic is of great significance for the development of high-performance OLEDs. Therefore, CzBT was doped into PVK as the light emitting layer in solution-processable OLED devices. The electroluminescence (EL) devices with the configuration of ITO/PEDOT:PSS/PVK:CzBT (20 wt%)/TPBI (40 nm)/LiF (1.4 nm)/Al (100 nm) (Figure 6a) were fabricated, and the optimized performances are shown in Figure 6. Here, poly(3,4-ethylenedioxythiophene)-poly(styrenesulfonate) (PEDOT:PSS) was used for hole injection, PVK was used as a hole transporting layer and host material, and 2,2′,2″-(1,3,5-benzinetriyl)-tris(1-phenyl-1-H-benzimidazole) (TPBI) was used as a hole blocking and electron transporting layer. The turn-on voltages (at 1 cd/m^2) of the EL device are 4.9 V. The current density-voltage-luminance curves (Figure 6b) indicate that both current density and brightness increase sharply with increasing voltage. In particular, the device exhibited outstanding efficiency with maximal current efficiency of 62.7 cd/A and external quantum efficiency of 19.9% at 9.3 V (Figure 6c), and peak brightness of 90,858 cd/m^2. The relatively small efficiency roll-off (62 cd/A@10,000 cd/m^2) is due to the RISC reducing the concentration of triplet excitons, thereby alleviating the device's efficiency roll-off. The normalized EL spectra (Figure 6d) of the device show bright green electroluminescence with maximum emission at 530 nm, similar to the photoluminescence spectra of CzBT. The excellent device performance indicates that CzBT can effectively utilize triplet excitons via moderate RISC, thereby promoting high device efficiency.

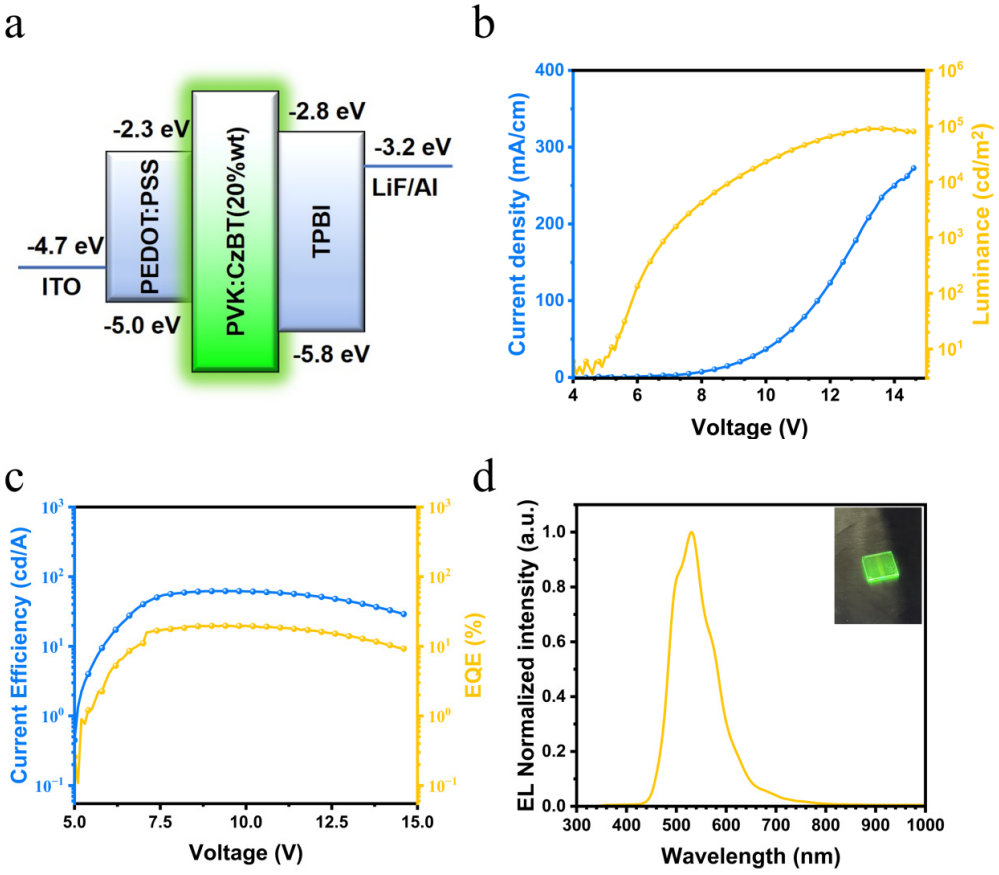

Figure 6. (**a**) Device configuration; (**b**) Current density-voltage-luminance characteristics of device; (**c**) Current efficiency and external quantum efficiency (EQE) as a function of voltage; (**d**) Normalized EL spectra.

3. Conclusions

In summary, polymers (NP1-10~NP1-1000) containing phosphor monomer with carbazole-benzothiazole structure in the side group were successfully synthesized and analyzed. The polymers with

high phosphor concentrations displayed TADF emission, while low phosphor concentrations showed RTP emission with lifetimes up to 240 ms, and high efficiency (up to 20%). Moreover, the dual emission features of the polymers enabled them to have color-tunable afterglows with delay time and feed ratios dependence. The theoretical calculations illustrated that the introduction of twisted D-A structure and heteroatoms improved SOC and resulted in RTP emission as well as TADF emission in aggregated states. Interestingly, the solution processable OLED device with CzBT doping in PVK as the emitting layer exhibited excellent performance of 62.7 cd/A and maximum external quantum efficiency of 19.9%, which was owing to the full utilizing of triplet excitons.

Supplementary Materials

The following supporting information can be found at: https://www.sciepublish.com/article/pii/1017, Scheme S1. The synthetic routes of monomer CzBT, and polymers NP1-10~NP1-1000. Figure S1: ^{1}H NMR spectra of monomer CzBT; Figure S2: ^{13}C NMR spectra of monomer CzBT; Figure S3: MALDI-TOF MS spectra of monomer CzBT; Figure S4: HPLC spectra of the monomer CzBT; Figure S5: FTIR spectra of the polymers NP1-100~NP1-1000; Figure S6: DSC curves of polymers NP1-50~NP1-1000; Figure S7: TGA curves of polymers NP1-50~NP1-1000; Figure S8: Delayed spectra (77 K) of monomer CzBT and polymer NP1-100 at room temperature; Figure S9: Temperature-dependent delay spectra of NP1-50; Figure S10: Excitation-dependent delay spectra of NP1-50; Figure S11: Delay spectra of polymers NP1-10~NP1-1000 with different concentrations under 380 nm excitation; Figure S12: CIE coordinate spectra of NP1-200 at different delay times; Figure S13: The fluorescent and delayed fluorescent spectra of CzBT:PVK (1:10). Table S1: Molecular weight of polymers; Table S2: Photophysical properties of polymers.

Acknowledgments

We gratefully acknowledge the financial support from the National Natural Science Foundation of China (NNSFC 22175149 and 62375085).

Author Contributions

H.W. executed the experiments and conducted a comprehensive analysis of the data. Y.G. was responsible for the lifetime tests and temperature-variable delayed spectra. Y.W. and F.W. conducted the OLED devices. C.W. helped analyze the experimental data. P.W. conceived and supervised the project, revised and finalized the manuscript. All contributors have given their approval for the submitted version of the manuscript.

Ethics Statement

Not applicable.

Informed Consent Statement

Not applicable.

Data Availability Statement

All data generated or analyzed during this study are included in this published article and its supplementary information files.

Funding

This research received no external funding.

Declaration of Competing Interest

The authors declare that they have no known competing financial interests or personal relationships that could have appeared to influence the work reported in this paper.

References

1. Fu Y, Liu H, Tang BZ, Zhao Z. Realizing efficient blue and deep-blue delayed fluorescence materials with record-beating electroluminescence efficiencies of 43.4%. *Nat. Commun.* **2023**, *14*, 2019. DOI:10.1038/s41467-023-37687-3
2. Kim HS, Cheon HJ, Lee SH, Kim J, Yoo S, Kim Y-H, et al. Advancing efficiency in deep-blue OLEDs: Exploring a machine learning–driven multiresonance TADF molecular design. *Sci. Adv.* **2025**, *11*, eadr1326. DOI:10.1126/sciadv.adr1326
3. Huang Z, Xie H, Miao J, Wei Y, Zou Y, Hua T, et al. Charge transfer excited state promoted multiple resonance delayed fluorescence emitter for high-performance narrowband electroluminescence. *J. Am. Chem. Soc.* **2023**, *145*, 12550–12560. DOI:10.1021/jacs.3c01267
4. Liu Y, Li C, Ren Z, Yan S, Bryce MR. All-organic thermally activated delayed fluorescence materials for organic light-emitting diodes. *Nat. Rev. Mater.* **2018**, *3*, 18020. DOI:10.1038/natrevmats.2018.20
5. Zhan L, Xu Y, Chen T, Tang Y, Zhong C, Lin Q, et al. Organic molecules with dual triplet-harvesting channels enable efficient X-ray scintillation and imaging. *Aggregate* **2024**, *5*, e485. DOI:10.1002/agt2.485
6. Dai M, Zhou B, Fang X, Yan D. Two-dimensional hybrid perovskitoid micro/nanosheets: Colorful ultralong phosphorescence, delayed fluorescence, and anisotropic optical waveguide. *ACS Appl. Mater. Interfaces* **2022**, *14*, 40223–40231. DOI:10.1021/acsami.2c11164
7. Chen X-K, Kim D, Brédas J-L. Thermally activated delayed fluorescence (TADF) path toward efficient electroluminescence in purely organic materials: Molecular level insight. *Acc. Chem. Res.* **2018**, *51*, 2215–2224. DOI:10.1021/acs.accounts.8b00174
8. Huang T, Jiang W, Duan L. Recent progress in solution processable TADF materials for organic light-emitting diodes. *J. Mater. Chem. C* **2018**, *6*, 5577–5596. DOI:10.1039/C8TC01139G
9. Uoyama H, Goushi K, Shizu K, Nomura H, Adachi C. Highly efficient organic light-emitting diodes from delayed fluorescence. *Nature* **2012**, *492*, 234–238. DOI:10.1038/nature11687
10. Zhang Q, Li J, Shizu K, Huang S, Hirata S, Miyazaki H, et al. Design of efficient thermally activated delayed fluorescence materials for pure blue organic light emitting diodes. *J. Am. Chem. Soc.* **2012**, *134*, 14706–14709. DOI:10.1021/ja306538w
11. Chan CY, Cui LS, Kim JU, Nakanotani H, Adachi C. Rational molecular design for deep-blue thermally activated delayed fluorescence emitters. *Adv. Funct. Mater.* **2018**, *28*, 1706023. DOI:10.1002/adfm.201706023
12. Yang Z, Mao Z, Xie Z, Zhang Y, Liu S, Zhao J, et al. Recent advances in organic thermally activated delayed fluorescence materials. *Chem. Soc. Rev.* **2017**, *46*, 915–1016. DOI:10.1039/C6CS00368K
13. Samanta PK, Kim D, Coropceanu V, Brédas J-L. Up-conversion intersystem crossing rates in organic emitters for thermally activated delayed fluorescence: Impact of the nature of singlet *vs*. triplet excited states. *J. Am. Chem. Soc.* **2017**, *139*, 4042–4051. DOI:10.1021/jacs.6b12124
14. Wu T-L, Huang M-J, Lin C-C, Huang P-Y, Chou T-Y, Chen-Cheng R-W, et al. Diboron compound-based organic light-emitting diodes with high efficiency and reduced efficiency roll-off. *Nat. Photonics* **2018**, *12*, 235–240. DOI:10.1038/s41566-018-0112-9
15. Cui L-S, Gillett AJ, Zhang S-F, Ye H, Liu Y, Chen X-K, et al. Fast spin-flip enables efficient and stable organic electroluminescence from charge-transfer states. *Nat. Photonics* **2020**, *14*, 636–642. DOI:10.1038/s41566-020-0668-z
16. Tang X, Cui L-S, Li H-C, Gillett AJ, Auras F, Qu Y-K, et al. Highly efficient luminescence from space-confined charge-transfer emitters. *Nat. Mater.* **2020**, *19*, 1332–1338. DOI:10.1038/s41563-020-0710-z
17. Hong X, Zhang D, Yin C, Wang Q, Zhang Y, Huang T, et al. TADF molecules with π-extended acceptors for simplified high-efficiency blue and white organic light-emitting diodes. *Chem* **2022**, *8*, 1705–1719. DOI:10.1016/j.chempr.2022.02.017
18. Wang X, Sun Y, Wang G, Li J, Li X, Zhang K. TADF-type organic afterglow. *Angew. Chem. Int. Ed.* **2021**, *60*, 17138–17147. DOI:10.1002/anie.202105628
19. Wang J, Yang Y, Li K, Zhang L, Li Z. Purely organic fluorescence afterglow: Visible-light-excitation, inherent mechanism, tunable color, and practical applications with very low cost. *Angew. Chem. Int. Ed.* **2023**, *62*, e202304020. DOI:10.1002/anie.202304020
20. Zhang X, Zeng M, Zhang Y, Zhang C, Gao Z, He F, et al. Multicolor hyperafterglow from isolated fluorescence chromophores. *Nat. Commun.* **2023**, *14*, 475. DOI:10.1038/s41467-023-36105-y

21. Hua T, Zhan L, Li N, Huang Z, Cao X, Xiao Z, et al. Heavy-atom effect promotes multi-resonance thermally activated delayed fluorescence. *Chem. Eng. J.* **2021**, *426*, 131169. DOI:10.1016/j.cej.2021.131169
22. Li Q, Wu Y, Yang Q, Wang S, Shao S, Wang L. Selenium-doped polycyclic aromatic hydrocarbon multiresonance emitters with fast reverse intersystem crossing for narrowband blue emission. *ACS Appl. Mater. Interfaces* **2022**, *14*, 49995–50003. DOI:10.1021/acsami.2c12017
23. Yuan WZ, Shen XY, Zhao H, Lam JW, Tang L, Lu P, et al. Crystallization-induced phosphorescence of pure organic luminogens at room temperature. *J. Phys. Chem. C* **2010**, *114*, 6090–6099. DOI:10.1021/jp909388y
24. Ma X-K, Liu Y. Supramolecular purely organic room-temperature phosphorescence. *Acc. Chem. Res.* **2021**, *54*, 3403–3414. DOI:10.1021/acs.accounts.1c00336
25. Yan X, Peng H, Xiang Y, Wang J, Yu L, Tao Y, et al. Recent advances on host–guest material systems toward organic room temperature phosphorescence. *Small* **2022**, *18*, 2104073. DOI:10.1002/smll.202104073
26. Wu H, Gu L, Baryshnikov GV, Wang H, Minaev BF, Ågren H, et al. Molecular Phosphorescence in Polymer Matrix with Reversible Sensitivity. *ACS Appl. Mater. Interfaces* **2020**, *12*, 20765–20774. DOI:10.1021/acsami.0c04859
27. Wu H, Baryshnikov GV, Kuklin A, Minaev BF, Wu B, Gu L, et al. Multidimensional Structure Conformation of Persulfurated Benzene for Highly Efficient Phosphorescence. *ACS Appl. Mater. Interfaces* **2021**, *13*, 1314–1322. DOI:10.1021/acsami.0c16338
28. Data P, Takeda Y. Recent advancements in and the future of organic emitters: TADF-and RTP-active multifunctional organic materials. *Chem. Asian J.* **2019**, *14*, 1613–1636. DOI:10.1002/asia.201801791
29. Lee OS, McKay AP, Cordes DB, Warriner SL, Gather MC, Zysman-Colman E. Simultaneous Multi-Resonant Thermally Activated Delayed Fluorescence and Room Temperature Phosphorescence from Biluminescent Nitrogen-Containing Indolocarbazoles. *Adv. Sci.* **2025**, *12*, e03175. DOI:10.26434/chemrxiv-2024-mm272
30. Song T, Liu H, Ren J, Wang Z. Achieving TADF and RTP with Stimulus-Responsiveness and Tunability from Phenothiazine-Based Donor–Acceptor Molecules. *Adv. Opt. Mater.* **2024**, *12*, 2301215. DOI:10.1002/adom.202301215
31. Zhan L, Chen Z, Gong S, Xiang Y, Ni F, Zeng X, et al. A simple organic molecule realizing simultaneous TADF, RTP, AIE, and mechanoluminescence: Understanding the mechanism behind the multifunctional emitter. *Angew. Chem.* **2019**, *131*, 17815–17819. DOI:10.1002/ange.201910719
32. Li M, Xie W, Cai X, Peng X, Liu K, Gu Q, et al. Molecular engineering of sulfur-bridged polycyclic emitters towards tunable TADF and RTP electroluminescence. *Angew. Chem. Int. Ed.* **2022**, *61*, e202209343. DOI:10.1002/anie.202209343
33. Wang Y, Gao M, Ren J, Liang J, Zhao Y, Fang M, et al. Exciplex-induced TADF, persistent RTP and ML in a host–guest doping system. *Mater. Chem. Front.* **2023**, *7*, 1093–1099. DOI:10.1039/D2QM01205G
34. Chen K, Jiang Y, Zhu Y, Lei Y, Dai W, Liu M, et al. Host to regulate the T_1–S_1 and T_1–S_0 processes of guest excitons in doped systems to control the TADF and RTP emissions. *J. Mater. Chem. C* **2022**, *10*, 11607–11613. DOI:10.1039/D2TC02167F
35. He Z, Huang Z, Li T, Song J, Wu J, Ma X. Achieving Tunable Monomeric TADF and Aggregated RTP via Molecular Stacking. *ACS Appl. Mater. Interfaces* **2024**, *16*, 54742–54750. DOI:10.1021/acsami.4c14265
36. Niu Y, Guan Y, Long C, Ren C, Lu J, Jin C, et al. A universal strategy for achieving dual cross-linked networks to obtain ultralong polymeric room temperature phosphorescence. *Sci. China Chem.* **2023**, *66*, 1161–1168. DOI:10.1007/s11426-022-1492-x
37. Yin Z, Gu M, Ma H, Jiang X, Zhi J, Wang Y, et al. Molecular engineering through control of structural deformation for highly efficient ultralong organic phosphorescence. *Angew. Chem.* **2021**, *133*, 2086–2091. DOI:10.1002/ange.202011830
38. Wang C, Qiao Q, Chi W, Chen J, Liu W, Tan D, et al. Quantitative design of bright fluorophores and AIEgens by the accurate prediction of twisted intramolecular charge transfer (TICT). *Angew. Chem.* **2020**, *132*, 10246–10258. DOI:10.1002/ange.201916357
39. Shi H, Song L, Ma H, Sun C, Huang K, Lv A, et al. Highly efficient ultralong organic phosphorescence through intramolecular-space heavy-atom effect. *J. Phys. Chem. Lett.* **2019**, *10*, 595–600. DOI:10.1021/acs.jpclett.8b03712
40. Yang L-L, Wang H, Zhang J, Wu B, Li Q, Chen J-Y, et al. Understanding the AIE phenomenon of nonconjugated rhodamine derivatives via aggregation-induced molecular conformation change. *Nat. Commun.* **2024**, *15*, 999. DOI:10.1038/s41467-024-45271-6
41. Baryshnikov G, Minaev B, Ågren H. Theory and calculation of the phosphorescence phenomenon. *Chem. Rev.* **2017**, *117*, 6500–6537. DOI:10.1021/acs.chemrev.7b00060
42. Yu L, Liu Y, Zhou D, Ni Z, Li S, Yang C. Aggregation-Induced Anti-Kasha Emission: Unraveling Multimodal Luminescence Mechanisms in a Single Molecule with Five Morphologies. *Aggregate* **2025**, *6*, e70075. DOI:10.1002/agt2.70075

43. Ghasemi M, Mahmoudi M, Gudeika D, Leitonas K, Simokaitiene J, Dabuliene A, et al. Effects of the change of isomers on room-temperature phosphorescence, thermally activated delayed fluorescence, and long persistent luminescence of organic hole-transporting materials with the selective potential for the application in electronic devices and optical sensors of oxygen. *Chem. Eng. J.* **2023**, *473*, 145004. DOI:10.1016/j.cej.2023.145004
44. Zhang Q, Tsang D, Kuwabara H, Hatae Y, Li B, Takahashi T, et al. Nearly 100% internal quantum efficiency in undoped electroluminescent devices employing pure organic emitters. *Adv. Mater.* **2015**, *27*, 2096–2100. DOI:10.1002/adma.201405474
45. Fan T, Liu Q, Zhang H, Wang X, Zhang D, Duan L. Enhancing Spin–Orbit Coupling in an Indolocarbazole Multiresonance Emitter by a Sulfur-Containing Peripheral Substituent for a Fast Reverse Intersystem Crossing. *Adv. Mater.* **2024**, *36*, 2408816. DOI:10.1002/adma.202408816